

## Fermi Surfaces of Thorium and Actinium\*

R. P. Gupta

*Institute for Atomic Research and Department of Physics, Iowa State University, Ames, Iowa 50010*

and

T. L. Loucks

*Science Center, North American Rockwell Corporation, Thousand Oaks, California 91360*

(Received 18 December 1969)

The results of a theoretical study of the energy bands and the Fermi surface of thorium calculated by the relativistic-augmented-plane-wave (RAPW) method and of actinium (rigid-band approximation) are reported. A muffin-tin version of the crystal potential was used and the exchange was included in the full  $\rho^{1/3}$  Slater approximation. A set of 36 reciprocal-lattice vectors was used in the expansion of the wave function, and with this set the energy eigenvalues were converged to within 0.003 Ry at the points of high symmetry. The calculated bands were interpolated by the method of "spline-fits" to obtain the density of states and the Fermi energy. The Fermi surface consists of three distinct pieces: a hole surface shaped like a rounded cube centered at  $\Gamma$ , electron surfaces shaped like pairs of lungs centered on the symmetry lines  $\Gamma K$ , and hole surfaces shaped like dumbbells centered on the symmetry lines  $\Gamma L$ . The de Haas-van Alphen frequencies are determined and the results compared with the existing experimental data. Assuming a rigid-band model, the present results have been used to predict the Fermi surface of actinium.

## I. INTRODUCTION

Our understanding of the electronic structure of metals has greatly increased during the past few years primarily due to the effort which has been devoted to the energy-band calculations and the experiments such as the de Haas-van Alphen (dHvA) effect, cyclotron resonance, etc., which can be related directly or indirectly to the geometry of the Fermi surface. From the results of the improved band calculations and related experiments a unified picture has emerged of the role played by conduction electrons, not only in simple metals but also in complicated metals of the transition series and even the rare earths. Although there have been no direct experiments like the dHvA effect performed to date on rare earths, there are other evidences which lend strong support to the existing band calculations on these metals.

The actinide series is generally much more complicated than the rare-earth series; however, thorium is probably one of the simplest of the actinides. The naturally occurring isotope of thorium has a half-life of  $1.39 \times 10^{10}$  years. It is a heavy element ( $Z=90$ ) which crystallizes in the face-centered-cubic (fcc) crystal structure at all temperatures of interest (below  $\approx 1400^\circ\text{C}$ ). It has a partially filled  $d$ -shell with free-atom configuration  $6d^2 7s^2$ , similar to the lighter elements Ti, Zr, and Hf except that they have the hexagonal-close-packed (hcp) structure. Like fcc lead, thorium also has four valence electrons but, from our present knowledge of the transition and rare-earth metals, it is hard to expect that the Fermi surface

of thorium will in any event resemble that of Pb which is almost free-electron-like. Very recently, experimental physicists have shown some interest in the study of actinides and the results of two dHvA measurements on thorium<sup>1-3</sup> are now available. This has greatly enhanced our interest in a theoretical study of the electronic structure of this metal.

The first theoretical study of the band structure of thorium was made by Lehman<sup>4</sup> 10 years ago. The method he used was similar to the Slater-Koster interpolation scheme in some respects. It was a parametrized model based upon Kohn's variational principle. Although he included the spin-orbit interaction, the calculation was limited to the  $d$  bands only. Recently, Keeton and Loucks<sup>5</sup> studied the energy bands of thorium by the augmented-plane-wave (APW) method, both with and without the relativistic effects. As expected, they concluded that the relativistic effects are large in thorium and the  $s$  band lies below the  $d$  bands, meaning that these two effects must be included in any calculation of the electronic properties of this metal.

It was only 2 years ago that the results of the first experiment on dHvA in thorium were published. Thorsen *et al.*<sup>1</sup> found that their results could be interpreted in terms of a model of the Fermi surface consisting of a nearly spherical piece at the center of the Brillouin zone and a set of six closed segments located along  $[100]$  axes at the symmetry points  $X$ . Their results could not be explained on the basis of either the free-electron model or the two existing band calculations. It is easy to understand why the free-electron

TABLE I. The potential used for thorium  $2Z_p(r) = -rV(r)$  (the factor of 2 arises since  $e^2 = 2$  a. u.).

$r$	$2Z_p(r)$	$r$	$2Z_p(r)$	$r$	$2Z_p(r)$
0.00020	179.79	0.01005	168.23	0.17378	82.91
0.00032	179.65	0.01168	166.50	0.20190	75.45
0.00043	179.52	0.01357	164.56	0.23458	68.03
0.00058	179.34	0.01576	162.38	0.27254	60.72
0.00078	179.09	0.01832	159.95	0.31665	53.62
0.00106	178.76	0.02128	157.25	0.36789	46.90
0.00143	178.30	0.02472	154.25	0.42743	40.69
0.00166	178.01	0.02873	150.94	0.49660	35.01
0.00193	177.68	0.03337	147.29	0.57697	29.90
0.00224	177.29	0.03878	143.27	0.67034	25.31
0.00261	176.85	0.04505	138.86	0.77882	21.14
0.00303	176.33	0.05234	134.05	0.90486	17.36
0.00352	175.73	0.06081	128.83	1.05130	14.00
0.00409	175.03	0.07065	123.23	1.22144	11.09
0.00475	174.24	0.08209	117.26	1.41911	8.60
0.00552	173.33	0.09537	110.96	1.64877	6.46
0.00641	172.29	0.11081	104.34	1.91560	4.58
0.00745	171.10	0.12874	97.43	2.22561	2.94
0.00865	169.76	0.14957	90.27	2.58578	1.57
				3.00425	0.53

model is inadequate, thorium being an element with both  $s$  and  $d$  electrons. It is also apparent from Lehman's article<sup>4</sup> that he chose not to include the  $s$  band since the primary emphasis was on the spin-orbit splitting; and one cannot expect complete information on the Fermi surface from such a calculation. But it is surprising, especially to those who have witnessed the numerous successful applications of the APW method to other metals, that the relativistic-augmented-plane-wave (RAPW) calculation of Keeton and Loucks<sup>5</sup> did not provide useful information on the Fermi surface of thorium.

The source of error in this particular case was pointed out by Waber.<sup>6</sup> He observed in the results published by Keeton and Loucks that the  $5f$  levels were in the middle of the conduction band. The authors had not taken this into account. As a result the Fermi surface based on these energy bands was essentially meaningless. In the present calculation this has been avoided by modifying the logarithmic derivative for the  $f$  orbitals so that no singularity exists in the energy range of interest. Previous experience on the rare earths indicates that this has little or no effect on the actual  $s$ - $d$  bands. The procedure is justified from a physical standpoint because the exact position of the  $5f$  levels is very sensitive to the potential and to intra-atomic interactions not included in the energy-band model. Experimental evidence indicates that the  $5f$  levels are well above the Fermi energy in thorium.

## II. DESCRIPTION OF CALCULATION

The crystal structure of thorium is fcc with the lattice constant  $a = 9.608$  a. u.<sup>7,8</sup> The crystal po-

tential was constructed using the method suggested by Mattheiss.<sup>9</sup> The relativistic self-consistent calculations of Libermann *et al.*<sup>10</sup> for the free-atom configuration  $6d^27s^2$  were used. Exchange was treated throughout using the Slater  $\rho^{1/3}$  approximation. The RAPW sphere radius was  $R = 3.1582$  a. u. and the zero of the energy was chosen such that the potential outside the sphere was zero. The potential is listed in Table I.

The energy bands were calculated using a basis set of 36 reciprocal-lattice vectors; these are listed in Table II. The notation used for these vectors is

$$(lmn) = (2\pi/a)(l\vec{i} + m\vec{j} + n\vec{k}),$$

where  $\vec{i}$ ,  $\vec{j}$ , and  $\vec{k}$  are the unit vectors along the  $x$ ,  $y$ ,

TABLE II. Reciprocal-lattice vectors used in RAPW expansion for all the points in the zone. They are listed in order of importance for the zone as a whole (based on  $\vec{k}_i = \vec{k} - \vec{K}_i$ ).

(0, 0, 0)	(1, 1, 1)	(0, 2, 0)
(1, 1, $\bar{1}$ )	( $\bar{1}$ , 1, 1)	( $\bar{1}$ , 1, $\bar{1}$ )
(2, 0, 0)	(0, 0, 2)	(1, $\bar{1}$ , 1)
( $\bar{1}$ , $\bar{1}$ , $\bar{1}$ )	( $\bar{1}$ , $\bar{1}$ , 1)	(1, $\bar{1}$ , $\bar{1}$ )
(2, 2, 0)	( $\bar{2}$ , 0, 0)	(0, 2, 0)
(0, 0, $\bar{2}$ )	(0, 2, 2)	(2, 0, 2)
( $\bar{2}$ , 2, 0)	(0, 2, $\bar{2}$ )	(1, 3, $\bar{1}$ )
(1, 3, 1)	( $\bar{1}$ , 3, 1)	( $\bar{1}$ , 3, $\bar{1}$ )
(3, 1, 1)	(3, 1, $\bar{1}$ )	(2, 0, $\bar{2}$ )
(2, 2, 2)	(1, 1, 3)	(2, 2, $\bar{2}$ )
( $\bar{2}$ , 0, $\bar{2}$ )	(0, $\bar{2}$ , $\bar{2}$ )	(2, 0, 2)
(0, $\bar{2}$ , 2)	(2, $\bar{2}$ , 0)	( $\bar{2}$ , 2, 0)

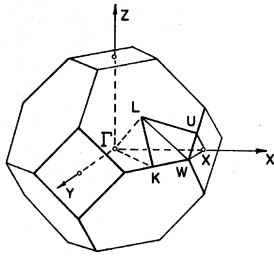


FIG. 1. Brillouin zone for the fcc crystal structure.

and  $z$ -axes, respectively. The eigenvalues at all symmetry points in the Brillouin zone (Fig. 1) were converged to within about 0.003 Ry using this set of vectors. The sum on  $\kappa^{11}$  was truncated at  $-8$  for the negative part of the sum and  $+7$  for the positive part. This means that orbital symmetries from  $l=0$  to  $7$  were included in the calculation.

The calculations were carried out on a discrete mesh within the first Brillouin zone. The whole of the Brillouin zone was partitioned into 2048 cubical-volume elements. Because of symmetry considerations this involves calculations only for 89 points lying within the  $\frac{1}{48}$ th zone which is irreducible under symmetry operations. The 89 points together with the first three energy bands are given in Table III. The bands are shown in Fig. 2.

### III. DENSITY OF STATES

The histogram of the density of states constructed from the calculated bands is shown in Fig. 3.  $\Delta E$  was taken to be 0.03 Ry. In order to find the density of states more accurately, the energy bands were interpolated throughout the Brillouin zone by the method of spline fits,<sup>12</sup> using appropriate boundary conditions. The histogram constructed in this way using a mesh of 2 048 000 points in the first Brillouin zone is shown in Fig. 4. The Fermi energy occurs at 0.595 Ry and the density of states at this energy is found to be 14.6 states/Ry atom. The energy of the lowest state at  $\Gamma$  is 0.197 Ry. This yields the width of the conduction band as 0.398 Ry.

There are several experimental measurements available on the electronic specific heat of thorium.<sup>13-16</sup> Clusius and Franzosini<sup>13</sup> found the electronic specific-heat coefficient  $\gamma = 16.4 \times 10^{-4}$  cal/mole deg<sup>2</sup>. Using the equation

$$\gamma = 0.828 \times 10^{-4} N(E_F) \text{ cal/mole deg}^2,$$

where  $N(E_F)$  is in states/Ry atom, this value of  $\gamma$  corresponds to  $N(E_F) = 19.8$  states/Ry atom. This would have to be corrected for electron-phonon enhancement before a rigorous comparison with a "band" density of states could be made, but

TABLE III. Energy bands of thorium (Ry).

$4ak/\pi$	Band 1	Band 2	Band 3
$\Gamma$ (0, 0, 0)	0.197	0.645	0.645
(1, 0, 0)	0.213	0.633	0.653
(2, 0, 0)	0.256	0.593	0.676
(3, 0, 0)	0.314	0.544	0.687
(4, 0, 0)	0.362	0.497	0.659
(5, 0, 0)	0.369	0.459	0.688
(6, 0, 0)	0.347	0.431	0.768
(7, 0, 0)	0.325	0.414	0.854
$X$ (8, 0, 0)	0.317	0.409	0.899
(1, 1, 0)	0.228	0.625	0.657
(2, 1, 0)	0.268	0.592	0.673
(3, 1, 0)	0.324	0.548	0.669
(4, 1, 0)	0.373	0.505	0.639
(5, 1, 0)	0.381	0.469	0.660
(6, 1, 0)	0.358	0.442	0.732
(7, 1, 0)	0.337	0.426	0.811
(8, 1, 0)	0.328	0.422	0.852
(2, 2, 0)	0.303	0.582	0.668
(3, 2, 0)	0.353	0.558	0.645
(4, 2, 0)	0.402	0.527	0.602
(5, 2, 0)	0.415	0.498	0.603
(6, 2, 0)	0.392	0.475	0.657
(7, 2, 0)	0.369	0.462	0.726
(8, 2, 0)	0.360	0.458	0.766
(3, 3, 0)	0.395	0.562	0.616
(4, 3, 0)	0.441	0.554	0.571
(5, 3, 0)	0.465	0.536	0.548
(6, 3, 0)	0.438	0.527	0.583
(7, 3, 0)	0.412	0.518	0.640
(8, 3, 0)	0.403	0.516	0.677
(4, 4, 0)	0.476	0.536	0.584
(5, 4, 0)	0.486	0.516	0.595
(6, 4, 0)	0.457	0.536	0.598
(7, 4, 0)	0.434	0.564	0.601
$W$ (8, 4, 0)	0.426	0.577	0.608
(5, 5, 0)	0.447	0.536	0.638
(6, 5, 0)	0.421	0.530	0.663
(7, 5, 0)	0.407	0.519	0.675
$K$ (6, 6, 0)	0.386	0.500	0.718
(1, 1, 1)	0.241	0.618	0.660
(2, 1, 1)	0.279	0.592	0.670
(3, 1, 1)	0.332	0.554	0.661
(4, 1, 1)	0.379	0.515	0.628
(5, 1, 1)	0.389	0.480	0.645
(6, 1, 1)	0.368	0.454	0.711
(7, 1, 1)	0.347	0.439	0.787
(8, 1, 1)	0.338	0.434	0.825
(2, 2, 1)	0.309	0.587	0.666
(3, 2, 1)	0.352	0.570	0.645
(4, 2, 1)	0.396	0.543	0.606
(5, 2, 1)	0.413	0.510	0.607
(6, 2, 1)	0.396	0.486	0.657
(7, 2, 1)	0.375	0.474	0.720
(8, 2, 1)	0.367	0.471	0.755
(3, 3, 1)	0.384	0.583	0.624
(4, 3, 1)	0.419	0.568	0.596
(5, 3, 1)	0.447	0.525	0.595
(6, 3, 1)	0.438	0.515	0.611

TABLE III. (continued)

$4ak/\pi$	Band 1	Band 2	Band 3
(7, 3, 1)	0.416	0.519	0.648
(8, 3, 1)	0.407	0.521	0.675
(4, 4, 1)	0.444	0.547	0.621
(5, 4, 1)	0.467	0.510	0.633
(6, 4, 1)	0.465	0.506	0.629
(7, 4, 1)	0.443	0.539	0.616
(5, 5, 1)	0.447	0.521	0.657
(6, 5, 1)	0.427	0.522	0.659
(2, 2, 2)	0.326	0.597	0.659
(3, 2, 2)	0.354	0.599	0.643
(4, 2, 2)	0.387	0.575	0.619
(5, 2, 2)	0.412	0.531	0.624
(6, 2, 2)	0.409	0.508	0.654
(7, 2, 2)	0.394	0.502	0.697
<i>U</i> (8, 2, 2)	0.386	0.502	0.721
(3, 3, 2)	0.365	0.623	0.637
(4, 3, 2)	0.387	0.588	0.648
(5, 3, 2)	0.416	0.538	0.654
(6, 3, 2)	0.434	0.512	0.656
(7, 3, 2)	0.427	0.522	0.660
(4, 4, 2)	0.399	0.572	0.659
(5, 4, 2)	0.423	0.534	0.675
(6, 4, 2)	0.457	0.496	0.667
(5, 5, 2)	0.429	0.523	0.681
(3, 3, 3)	0.359	0.627	0.660
(4, 3, 3)	0.369	0.606	0.650
(5, 3, 3)	0.395	0.560	0.665
(6, 3, 3)	0.429	0.523	0.683
(4, 4, 3)	0.369	0.603	0.642
(5, 4, 3)	0.388	0.571	0.653
<i>L</i> (4, 4, 4)	0.358	0.613	0.644

agreement with our value of 14.6 is nevertheless satisfactory. Smith and Walcott<sup>14</sup> had previously measured  $\gamma = 11.2 \times 10^{-4}$  cal/mole deg<sup>2</sup>. This would give  $N(E_F) = 13.5$  states/Ry atom. Clusius and Franzosini<sup>13</sup> attribute the disagreement with the results of Smith and Walcott<sup>14</sup> to differences in the purity of the two samples.

Very recently, Gordon *et al.*<sup>15</sup> and Decker and

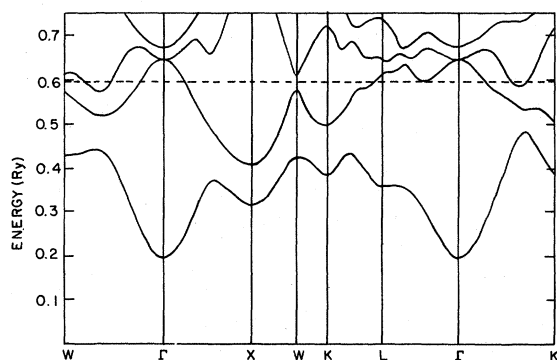


FIG. 2. Energy bands of thorium.

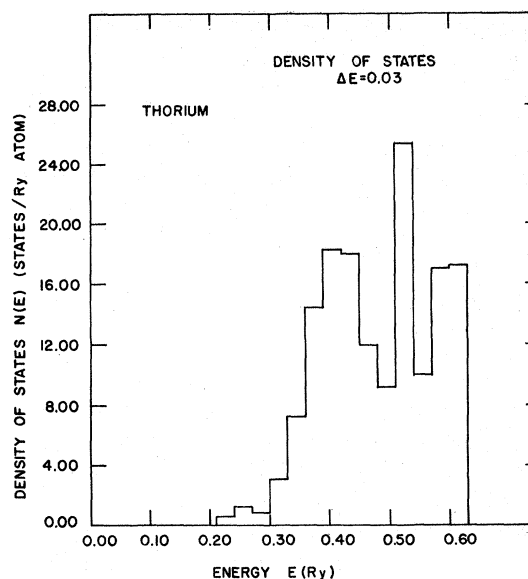


FIG. 3. Density-of-states curve for thorium. Total number of points in the Brillouin zone is equal to 2048.

Finnemore<sup>16</sup> also estimated the value of  $\gamma$  from superconductivity measurements. Both got essentially the same result of  $\gamma = 10.4 \times 10^{-4}$  cal/mole deg<sup>2</sup>. The corresponding density of states is 12.6 states/Ry atom, very close to our theoretical value. This value is much lower than the one observed by Clusius and Franzosini<sup>13</sup> but is only slightly smaller than the value of Smith and

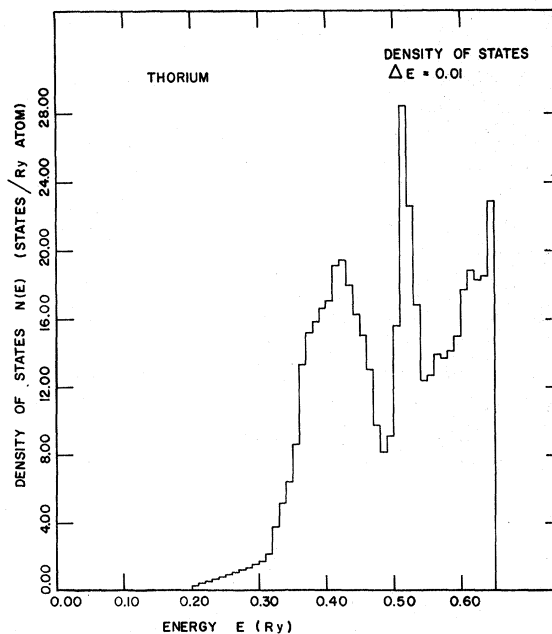


FIG. 4. Density-of-states curve for thorium. Total number of points in the Brillouin zone is equal to 2 048 000

Walcott,<sup>14</sup> The discrepancy has been attributed to the fact that the techniques used in the earlier experiments are less reliable.

The magnetic susceptibility has been measured by Smith and Greiner<sup>17</sup> from 130 – 300 °K and was found to be constant in that range and of magnitude  $0.41 \times 10^{-6}$  emu/g. For the purpose of making a rough comparison, we shall assume that the only contribution is the paramagnetic spin susceptibility. Using the equation

$$\chi = 0.0205 \times 10^{-6} N(E_F) \text{ emu/g ,}$$

we obtain  $N(E_F) = 20$  states/Ry atom, which is also in satisfactory agreement with our value. Since the measured  $\chi$  also contains diamagnetic contributions which are negative, the paramagnetic part of the susceptibility will be somewhat larger and hence, so will the resulting value of  $N(E_F)$ .

It must be pointed out that the experimental results are so much at variance among themselves that is difficult to draw any firm conclusion about the density of states in thorium. The latest superconductivity data,<sup>16</sup> however, would lead to the conclusion that the electron-phonon interactions are small in thorium since the experimental den-

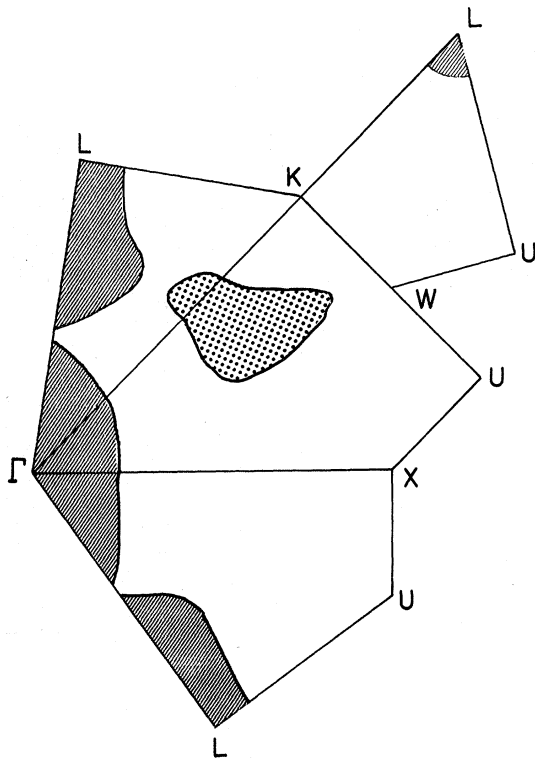


FIG. 5. Intersections of the Fermi surface of thorium with the symmetry planes in the Brillouin zone. The electrons are shown dotted and the holes lined.

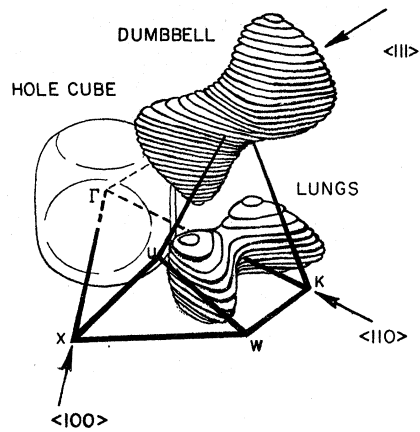


FIG. 6. Fermi surface of thorium.

sity of states is almost equal to the “band” density of states.

#### IV. FERMI SURFACE

Intersections of the Fermi surface with the symmetry planes of the Brillouin zone are shown in Fig. 5. The Fermi surface is shown in Fig. 6. It consists of three distinct pieces: a hole surface at the center of the Brillouin zone shaped like a rounded cube, electron surfaces on symmetry lines  $\Gamma K$   $\langle 110 \rangle$  shaped like pairs of lungs, and the hole surfaces on the symmetry lines  $\Gamma L$   $\langle 111 \rangle$  shaped like dumbbells with triangular ends. The dHvA frequencies have been calculated on the basis of this model. The frequencies are related to the extremal cross-sectional areas by the relation

$$f = 374.1 \times 10^6 A \text{ (G),}$$

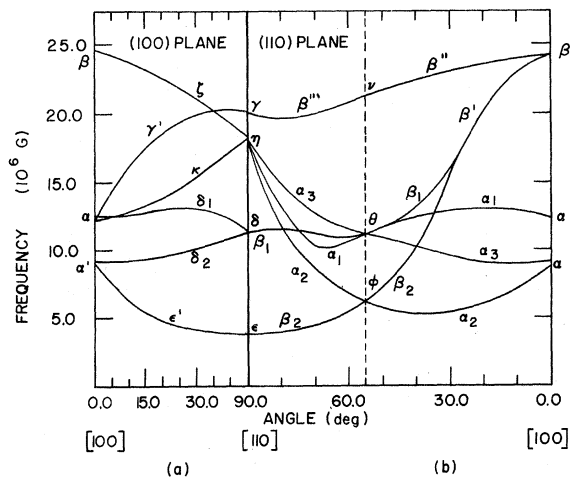


FIG. 7. The dHvA frequencies calculated from the electron surface.

where  $A$  is the area of an extremal orbit in a.u.<sup>-2</sup>. The angular dependence of the dHvA frequencies in the (100) and (110) planes predicted by this model is shown in Figs. 7 and 8 for the electron and the hole surfaces, respectively.

The cyclotron effective masses (as a fraction of the electron rest mass) have also been calculated for some of the orbits and are listed in Table IV. The relation

$$m^*/m = 0.3183\Delta A/\Delta E$$

was used, where  $\Delta A$  is the change in the extremal area of an orbit (a.u.<sup>-2</sup>) corresponding to an energy change  $\Delta E$  (Ry).

We first examine the behavior of the extremal areas generated by the 12 segments of the electron surface. For a given field direction, each of these segments will give rise to one or more extremal areas. The extremal areas produced by two segments can be the same or different depending upon their orientations with the field. To obtain the extremal areas arising from all the segments for a given field direction in a given plane, we need not study all the segments simultaneously. For reasons of symmetry we can alternatively choose a single segment, say the one

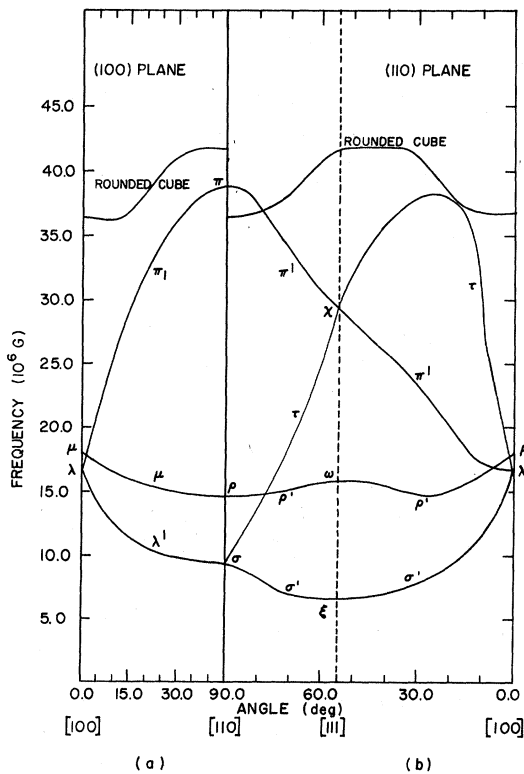


FIG. 8. The dHvA frequencies calculated from the

TABLE IV. Predicted and observed dHvA frequencies in symmetry directions.

Surface	Direction	Predicted frequency (MG)	Observed frequency (MG)	Predicted effective mass ( $m^*/m$ )	
Lungs	[100]	$\alpha'$ 8.8	10.0	0.40	
		9.1		0.37	
		12.0		0.47	
		$\alpha$ 12.2		11.9	0.59
		12.4		0.41	
	[110]	$\beta$ 24.4	22.1	0.55	
		$\epsilon$ 3.8	2.0	0.23	
		$\delta$ 11.3	9.6	0.42	
	[111]	$\eta$ 18.1		0.62	
		$\gamma$ 20.1	19.9	0.40	
$\phi$ 6.3					
$\theta$ 11.3		11.7			
Dumbbell	[100]	$\nu$ 21.4	22.5		
		$\lambda$ 16.8			
	[110]	$\mu$ 18.0			
		$\sigma$ 9.4	10.9		
		$\rho$ 14.8			
	[111]	$\pi$ 38.9			
		$\xi$ 6.7	10.9		
		$\omega$ 15.9			
		$\chi$ 29.7			
	Rounded cube	[100]	36.5	22.1	
[110]		41.8	24.8		
[111]		41.5	24.8		

centered along [110], and study the extremal areas produced by this segment when the field is rotated in the appropriate set of planes. For example, the behavior of all 12 surfaces with respect to the magnetic field in (100) plane will be the same as the behavior of the surface centered along [110] with the rotation of the field in the (001) and (100) planes. Similarly, the behavior of all the 12 surfaces in (110) plane can be obtained by examining the surface along [110] when the field is rotated in (110), ( $\bar{1}\bar{1}0$ ), and (011) planes.

Considering the magnetic field in the (001) plane, we find five extremal areas for [100] direction which essentially fall into two groups. The group denoted by  $\alpha$  has three extremals which have frequencies around 12 MG ( $12 \times 10^6$  G). The second group having two frequencies close together is denoted by  $\alpha'$  and falls around 9 MG. The individual frequencies of these extremals are given in Table IV. As the direction is changed from [100] toward  $[\bar{1}\bar{1}0]$ , the separation between the two frequencies at  $\alpha'$  increases and the lower frequency finally ends up as  $\epsilon$  and the higher one as  $\delta$  in the  $[\bar{1}\bar{1}0]$  direction. Only one of the frequencies at  $\alpha$  follows  $\delta_1$  and is shown as  $\delta$  in  $[\bar{1}\bar{1}0]$  direction. The two other frequencies disappear. On the other hand,

if we move toward the  $[110]$  direction the frequencies at  $\alpha'$  are not seen and only the one from  $\alpha$  is found to survive. This frequency rises sharply along  $\gamma'$  and is represented by  $\gamma$  in  $[110]$ . The frequency branches  $\xi$  and  $\kappa$  are obtained when the field is rotated toward  $[011]$  in the  $(100)$  plane from the  $[001]$  and  $[010]$  directions, respectively.

The situation is slightly more complicated for the  $(110)$  plane. In the plane  $(011)$ , we again get the group of frequencies  $\alpha$  and  $\alpha'$  in  $[100]$  direction as expected. As the field is rotated toward  $[0\bar{1}1]$ , the two frequencies at  $\alpha'$  follow the path  $\alpha_3$  and  $\alpha_2$  and again two of the frequencies at  $\alpha$  disappear and only one of them is found to trace the route of  $\alpha_1$ . The three frequencies  $\alpha_1$ ,  $\alpha_2$ , and  $\alpha_3$  merge in  $[0\bar{1}1]$  direction and only one frequency  $\eta$  is obtained.  $\alpha_1$  and  $\alpha_3$  cross also in  $[\bar{1}\bar{1}1]$  direction and a single orbit  $\theta$  is found. In the  $(1\bar{1}0)$  plane, the branch  $\beta\beta''\gamma$  is followed for a magnetic field rotating from  $[001]$  to the  $[110]$  direction. But if the plane  $(110)$  is considered, the frequency  $\beta$  in  $[001]$  direction follows  $\beta'$  to about  $28^\circ$  as one moves toward  $[\bar{1}\bar{1}0]$  and then splits into two separate frequencies  $\beta_1$  and  $\beta_2$  which are shown as  $\delta$  and  $\epsilon$  in  $[\bar{1}\bar{1}0]$ .  $\beta_1$  crosses with  $\theta$  and  $\beta_2$  with  $\phi$  in  $[\bar{1}\bar{1}1]$  direction.

The extremal areas on the hole surfaces are similarly obtained. There is only one extremal area for the rounded cube for a given field direction in  $(100)$  or  $(110)$  plane. The dumbbell, however, gives rise to several orbits in any given direction. If we confine ourselves to the dumbbell centered along  $[111]$ , we find two frequencies  $\lambda$  and  $\mu$  in the  $[001]$  direction. As one moves away from  $[001]$  toward  $[101]$  in the  $(010)$  plane, both the extremals start decreasing but the rate is larger in the case of  $\lambda$ . These extremals are shown as  $\sigma$  and  $\rho$  in the  $[101]$  direction. However, if instead one moves toward  $[\bar{1}01]$ , then the orbit  $\mu$  disappears and only  $\lambda$  is seen. It increases rapidly and is denoted by  $\pi$  in  $[\bar{1}01]$  direction. Similarly, if the direction of the magnetic field is changed from  $[001]$  toward  $[110]$  in the  $(1\bar{1}0)$  plane, the frequency  $\mu$  approaches slowly toward  $\rho$  and  $\lambda$  decreases until it reaches  $\xi$  in the  $[111]$  direction and then slowly increases to reach  $\sigma$  in the  $[110]$  direction. But if we move from  $[001]$  toward  $[\bar{1}\bar{1}0]$  in the  $(110)$  plane, the frequency  $\mu$  disappears altogether and  $\lambda$  rises very sharply, and in  $[\bar{1}\bar{1}0]$  it is shown as  $\pi$ . Yet another possible choice is to start from  $[00\bar{1}]$  toward  $[110]$  in the  $(1\bar{1}0)$  plane in which case the frequency  $\lambda$  rises sharply to a value of 38 MG at about  $25^\circ$  from  $[00\bar{1}]$  and then drops sharply to the value  $\sigma$  in  $[110]$ .

## V. COMPARISON WITH EXPERIMENT

As already pointed out, there are two sets of experimental data<sup>1-3</sup> with which correlation of our

Fermi-surface results is possible. The crystal used by Thorsen *et al.*<sup>1</sup> was of relatively poor quality, and a great difficulty was experienced in resolving various frequency branches in their experiment. It was therefore difficult for them to provide a unique interpretation of their results. The sample used by Boyle and Gold<sup>2,3</sup> was of much higher purity, and they also used a considerably improved experimental technique. An important feature of their results is that they were able to resolve their data into distinct frequency branches. Broadly speaking, most of their data also fall into two relatively narrow bands of 9.5–14 and 19–25 MG, as found earlier by Thorsen *et al.*; in addition, a low-frequency branch  $\approx 2.5$  MG was also detected. We shall compare our model with the data of Boyle and Gold which are more extensive than those of Thorsen *et al.* Their results are shown in Fig. 9.

We shall first compare the results in the  $(110)$  plane. We notice that the variation in the frequency of the branch  $F_1$  from the experiment is very small for small values of the angle  $\theta$  (measured from  $[110]$ ) but for large angles  $F_1$  increases rapidly. This behavior is well represented by the frequency branch  $\beta_1$  [Fig. 7(b)] obtained from the electron surface.  $\beta_1$  shows little variation for small angles but increases sharply for  $\theta > 35^\circ$ . It has a frequency of the order of 10 MG in the  $[110]$  direction and goes to about 14 MG at  $50^\circ$  from  $[110]$ , a variation observed with  $F_1$ . We therefore associate  $F_1$  with  $\beta_1$ . The branch  $F_2'$  exhibits a minimum at  $[111]$  and increases faster than the inverse of the cosine of the angle from  $[111]$ . This suggests that this branch originates because of

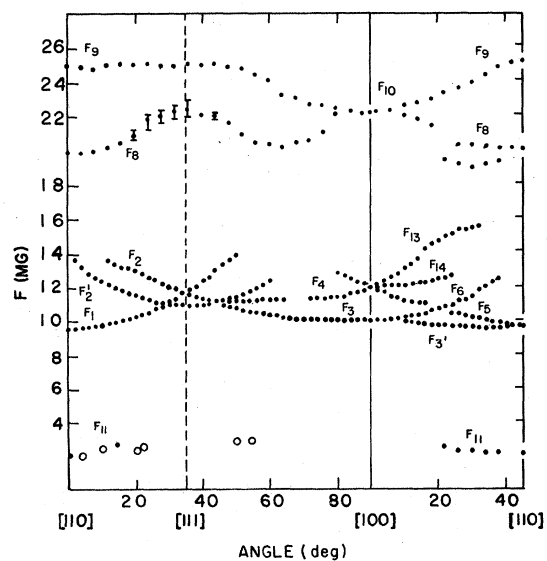


FIG. 9. The dHVA frequencies observed by Boyle and Gold experimentally.

the dumbbell-shaped portion of the Fermi surface. We therefore identify  $F_2'$  with the frequency branch  $\sigma'$  [Fig. 8(b)] from our calculation.

The frequency branch  $F_2$  decreases slowly in magnitude as one moves away from [110] and is then seen to split into two components,  $F_3$  and  $F_4$ , at about  $42^\circ$  from [110]. Near [100], the lower branch  $F_3$  is nearly flat while  $F_4$  increases in frequency as it approaches [100]. This behavior of  $F_2$ ,  $F_3$ , and  $F_4$  is predicted by  $\alpha_1$  and  $\alpha_3$  on the electron surface [Fig. 7(b)]. From [110] to [111],  $\alpha_3$  can be identified with  $F_2$  and thereafter  $F_3$  and  $F_4$  can be identified with  $\alpha_3$  and  $\alpha_1$ , respectively. The behavior of the branch  $F_8$  is very much the same as is found with  $\beta''$  [Fig. 7(b)].

The angular variation of the frequency of the branch  $F_9$  shows that  $F_9$  is obviously due to the rounded cube located at the center of the Brillouin zone. The calculated frequencies from this piece of the Fermi surface are, however, about 50% higher than those observed. This suggests that the dimensions of the rounded cube be reduced to about  $\frac{2}{3}$  of the present size.

In the (100) plane, the most striking feature of the experimental data is that the three branches  $F_{13}$ ,  $F_{14}$ , and  $F_5$  meet in [100] direction. This character is predicted by our model also where  $\gamma'$ ,  $\kappa$ , and  $\delta_1$  [Fig. 7(a)] arising from the electron surface meet in  $\alpha$  in the [100] direction.  $\alpha$ , however, represents a group of three frequencies very close together, as already pointed out, but the separation is too small to be detected experimentally. Also,  $F_5$  and  $F_3'$  meet at [110]; so do  $\delta_1$  and  $\delta_2$  at  $\delta$  in [110]. We therefore conclude that the branches  $F_{13}$ ,  $F_{14}$ ,  $F_5$ , and  $F_3'$  arise from the geometry of the electron surface and can be associated with  $\gamma'$ ,  $\kappa$ ,  $\delta$ , and  $\delta_2$ , respectively, calculated from our model. The frequency branch  $F_8$  is assigned to  $\mu'$  [Fig. 8(a)] which shows the

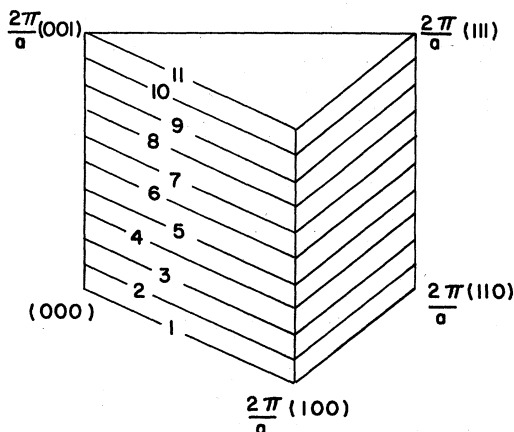


FIG. 10. Triangular prism in reciprocal space.

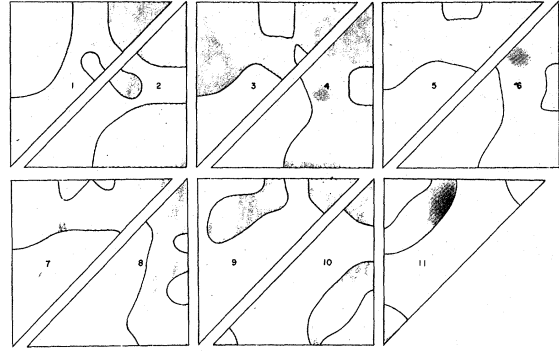


FIG. 11. Intersections of the Fermi surface of actinium with the planes of the triangular prism shown in Fig. 10.

same behavior but has lower frequencies. We could not find any proper assignment for  $F_6$  in terms of our model.  $F_9$  is again obviously due to the rounded hole cube at the center of the zone.

The experimental points represented by  $F_{11}$  in (100) and (110) planes can not be associated with any particular branch from the theory. Nonetheless, our model also predicts the existence of some lower frequency branches both in (100) and (110) planes. A numerical comparison between the predicted and the observed results is shown in Table IV.

## VI. FERMI SURFACE OF ACTINIUM

We have also calculated the Fermi surface of actinium ( $6d7s^2$ ) in the rigid-band approximation. The Fermi energy for actinium was found to be 0.525 Ry. The density of states for this value of  $E_f$  (Fig. 4) is 22.6 states/Ry atom which gives the electronic specific-heat coefficient

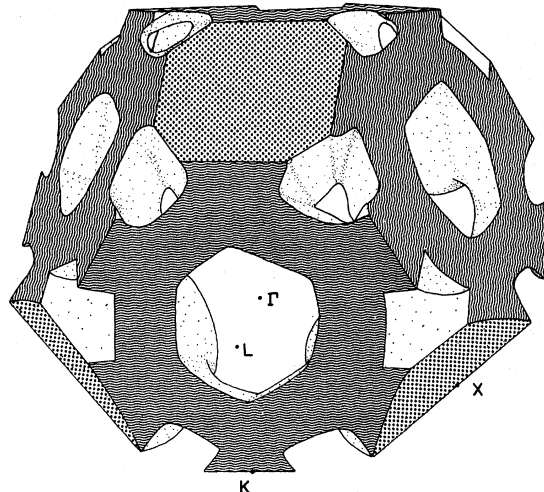


FIG. 12. Model of the Fermi surface of actinium.



$\gamma = 18.7 \times 10^{-4}$  cal/mole deg<sup>2</sup>.

In order to find out the intersections of the Fermi surface, a triangular prism of height  $\pi/a$  was chosen in reciprocal space, as shown in Fig. 10. The base of the prism was an isosceles right-angle triangle with its equal sides equal to  $2\pi/a$ . The volume of the prism was thus one-eighth of the Brillouin zone. The entire prism was divided into 11 equally distant layers, as shown in Fig. 10. The intersections of the Fermi surface with each of these layers are shown in Fig. 11, and a model of the Fermi surface is shown in Fig. 12. It is found to be a multiply connected surface. We are not aware of any experimental data on this metal with which the interpretation of these results is possible. Nevertheless, these results are in agreement with the recent calculation of Myron and Liu<sup>18</sup> for fcc La and Pr which have the same outer electron configuration as Ac.

## VII. CONCLUSION

We wish to point out that our model is only in

qualitative agreement with the experimental results of Boyle and Gold.<sup>2,3</sup> In general, the orbits derived from the electron surface yield frequencies which show reasonable quantitative agreement, but the frequencies from the dumbbell are smaller and the rounded cube larger than those observed. The discrepancy could be removed by scaling the entire hole surface to fit the experimental data. The results of our study, though only in qualitative agreement with experiment, are quite important because we now know that the lighter actinides which do not have 5f bands near the Fermi energy are similar to the transition metals and can be described by the same hybridized *s-d* energy band model.<sup>19</sup>

## ACKNOWLEDGMENTS

The authors are grateful to Dr. A. V. Gold, Dr. D. J. Boyle, Dr. S. K. Sinha, and Dr. S. H. Liu for helpful discussions during the course of present investigations. Thanks are due to Dr. D. J. Boyle for a critical reading of the manuscript.

\*Work performed in part in the Ames Laboratory of the U. S. Atomic Energy Commission, contribution No. 2655.

<sup>1</sup>A. C. Thorsen, A. S. Joseph, and L. E. Valby, Phys. Rev. **162**, 574 (1967).

<sup>2</sup>D. J. Boyle, Ph. D. thesis, Iowa State University, 1968 (unpublished).

<sup>3</sup>D. J. Boyle and A. V. Gold, Phys. Rev. Letters **22**, 461 (1969).

<sup>4</sup>G. W. Lehman, Phys. Rev. **116**, 846 (1959).

<sup>5</sup>S. C. Keeton and T. L. Loucks, Phys. Rev. **146**, 429 (1966).

<sup>6</sup>J. T. Waber (private communication).

<sup>7</sup>R. W. G. Wyckoff, *Crystal Structures* (Interscience, New York, 1963), Vol. 1.

<sup>8</sup>We have used atomic units (a. u.) in which  $e^2=2$ ,  $m=\frac{1}{2}$ , and  $\hbar=1$ . Energies are in Ry (13.605 eV) and distances are in Bohr radii (0.5292 Å).

<sup>9</sup>L. F. Mattheiss, Phys. Rev. **133**, A1399 (1964).

<sup>10</sup>D. Liberman, J. T. Waber, and D. T. Cromer, Phys. Rev. **137**, A27 (1965).

<sup>11</sup> $\kappa$  is related to the orbital angular momentum quantum number, T. L. Loucks, *Augmented-Plane-Wave Method* (Benjamin, New York, 1967).

<sup>12</sup>R. H. Pennington, *Introductory Computer Methods and Numerical Analysis* (MacMillan, New York, 1965).

<sup>13</sup>K. Clusius and P. Franzosini, Z. Naturforsch. **11a**, 957 (1956).

<sup>14</sup>P. L. Smith and N. M. Walcott, *Conférence de Physique des Basses Températures, Paris*, 1955 (l'Institut International du Froid, Paris, 1955).

<sup>15</sup>J. E. Gordon, H. Montgomery, R. J. Noer, G. R. Pickett, and R. Torbon, Phys. Rev. **152**, 432 (1966).

<sup>16</sup>W. R. Decker and D. K. Finnemore, Phys. Rev. **172**, 430 (1969).

<sup>17</sup>J. F. Smith and J. D. Greiner, Phys. Rev. **115**, 884 (1959).

<sup>18</sup>H. W. Myron and S. H. Liu, Phys. Rev. B **1**, 2414 (1970).

<sup>19</sup>R. P. Gupta and T. L. Loucks, Phys. Rev. Letters **22**, 458 (1969).